Electronic Supplementary Information (ESI)

Calixarene-coated gold nanorods as robust photothermal agents

Victor Lepeintre,[a,b] Franck Camerel,[c] Corinne Lagrost,[c,d] Maurice Retout,[a] Gilles Bruylants*[a] and Ivan Jabin*[b]

[a] Engineering of Molecular NanoSystems, Ecole Polytechnique de Bruxelles, Université libre de Bruxelles (ULB), avenue F. D. Roosevelt 50, CP165/64, B-1050 Brussels, Belgium.

[b] Laboratoire de Chimie Organique, Université libre de Bruxelles (ULB), Avenue F. D. Roosevelt 50, CP160/06, B-1050 Brussels, Belgium.

[c] Univ Rennes, CNRS, ISCR – UMR 6226, F-35000 Rennes, France.

[d] Univ Rennes, CNRS, ScanMAT – UAR 2025, F-35000 Rennes, France.

* Corresponding authors: Ivan.Jabin@ulb.be; Gilles.Bruylants@ulb.be

Table of Contents

Supplementary Methods

General Materials

Hexadecyltrimethylammonium bromide (CTAB, $\geq$ 99%), silver nitrate (AgNO$_3$, $\geq$ 99.8%), L-ascorbic acid ($\geq$ 99%) and dimethyl sulfoxide (DMSO, $\geq$ 99.9%) were purchased from VWR. Sodium borohydride (NaBH$_4$, 99%), Gold(III) chloride hydrate (HAuCl$_4$·xH$_2$O, 99.995%), 1-decanol (n-decanol, for synthesis), hydrochloric acid (HCl, 1 M aqueous solution), sodium chloride (NaCl, for analysis), sodium hydroxide (NaOH, pellets for analysis), trisodium citrate dihydrate (Na$_3$C$_6$H$_5$O$_7$·2H$_2$O, for analysis), poly(sodium 4-styrenesulfonate) (PSS, M$_w$ $\approx$ 70000 Da), 1-ethyl-3-(3-dimethylaminopropyl)carbodiimide hydrochloride (EDC·HCl, BioXtra) and 2-(N-morpholino)ethanesulfonic acid monohydrate (MES, $\geq$ 99.5%) were purchased from Merck. Sodium N-hydroxysulfosuccinimide (sulfo-NHS, 99%) was purchased from Apollo Scientific. Potassium fluoride (KF, 99%) was purchased from Thermo Fisher Scientific. Alpha-thio-omega-(propionic acid) octa(ethylene glycol) (HS–PEG$_8$–COOH, M$_w$ = 459 Da) was purchased from Iris Biotech. Cyanine5.5 amine was purchased from Lumiprobe. Calix[4]arene X$_4$C$_4$(N$_2^+$)$_4$ was purchased from X4C. Milli-Q grade water (resistivity 18.2 MW cm at 25 °C) was used in all experiments. All glassware and Teflon-coated stir bars were cleaned with aqua regia (HCl/HNO$_3$ in 3:1 v/v) and rinsed thoroughly with water before usage. Aqua regia is highly toxic and corrosive and should only be handled in a fume hood with proper personal protective equipment. Caution! Although we have not encountered any problem, it is noted that diazonium salt derivatives are potentially explosive and should be handled with appropriate precautions.

AuNR synthesis

AuNR-CTAB were synthesized with a 3-step protocol described by González-Rubio *et al.*[1]

First step: synthesis of spherical gold seeds (1-2 nm)

To 10 mL of a CTAB (50 mM in water) and 1-decanol (13.5 mM in water) solution at 25 °C under stirring, 100 µL HAuCl$_4$ (50 mM in water) followed by 50 µL L-ascorbic acid (100 mM in water) were added, the solution became colourless. After 2 minutes, 400 µL of freshly prepared ice-cold NaBH$_4$ (20 mM in water) was added at once under vigorous stirring (1000 rpm) at 25 °C, the solution became brownish. The mixture was further stirred for 30 s and left undisturbed for 1 h at 25 °C before using.

Second step (symmetry breaking): synthesis of small anisotropic seeds

To 60 mL of a CTAB (50 mM in water) and 1-decanol (13.5 mM in water) solution at 25°C under stirring, 480 µL $AgNO_3$ (10 mM in water), 4.2 mL HCl (1 M in water), 600 µL $HAuCl_4$ (50 mM in water), and 780 µL L-ascorbic acid (100 mM in water) were sequentially added. Then, 3.6 mL of the spherical gold seed suspension was added under stirring and the mixture was further stirred for 30 s before being left undisturbed for 4 h at 25 °C. The solution changed from colourless to grey and finally black. The longitudinal LSPR band of the anisotropic seeds should be located at 725–730 nm at this point. The suspensions were then centrifuged at 21 130g for 1 h in 1.5 mL centrifuge tubes. The supernatants were discarded and pellets were resuspended with a total of 1.5 mL CTAB (10 mM in water). The concentrated gold anisotropic seed solution was then centrifuged twice more under the same conditions. Finally, the Au^0 concentration was fixed to 4.65 mM (OD_{400} = 10, optical path of 1 cm) by dilution with CTAB (10 mM in water). The obtained small anisotropic seed suspension is stable at room temperature while protected from light for at least several months.

Third step (growth): synthesis of AuNR-CTAB

Here is described a synthetic procedure for AuNR-CTAB with a target longitudinal LSPR band located around 850 nm, other target longitudinal LSPR band wavelengths can be obtained by varying the synthetic conditions.[1] To 10 mL of a CTAB (50 mM in water) and 1-decanol (11 mM in water) solution at 28 °C under stirring, 200 µL $AgNO_3$ (10 mM in water) and 100 µL $HAuCl_4$ (50 mM in water) were added, leading to a yellow solution. Then, 80 µL L-ascorbic acid (100 mM in water) was added, and the solution became colourless. 460 µL HCl (1 M in water) was then added followed by 50 µL of the small gold anisotropic seed suspension. The mixture was further stirred for 30 s before being left undisturbed for at least 4 h at 28 °C. The AuNR suspension was then centrifuged at 12 000g for 20 min, the supernatant was discarded and the pellet was resuspended with 10 mL of CTAB (1 mM in water). The suspension was then centrifuged once more under the same conditions, and the pellet was redispersed with 10 mL of CTAB (0.1 mM in water), affording the suspension of AuNR-CTAB with a longitudinal LSPR band located around 850 nm.

Instrumentation

UV-vis Absorption Spectroscopy

The optical absorption measurements were recorded from 1100 nm to 300 nm with a UV-vis-NIR spectrophotometer (Shimadzu, UV-1900) in disposable PMMA cuvette or quartz cuvettes.

Attenuated Total Reflection Fourier-Transform Infrared

Attenuated total reflection Fourier-transform infrared (ATR-FTIR) spectra were recorded at 70 °C on a Shimadzu QATR-S FTIR spectrophotometer. The AuNRs were centrifuged, and 5 µL of the pellet was deposited on the diamond crystal. Water was evaporated by heating the puck to 70 °C. Bare diamond was used for the background spectrum. LabSolutions IR software was used to record 128 scans. Data were processed and analysed using the LabSolutions IR software by correcting the baseline, setting apodization at 10 cm^{-1}, and normalizing on the most intense signal.

Transmission Electron Microscopy, Selected Area Electron Diffraction and Energy-Dispersive X-ray Spectroscopy

AuNRs (5 µL, ~1 nM) were deposited on a carbon-coated 200 square-mesh nickel grid (placed on Parafilm), and the droplet was then allowed to dry at room temperature. Transmission electron microscopy (TEM) images and selected area electron diffraction (SAED) patterns of the AuNRs were obtained with a Jeol JEM 2100 HR transmission electron microscope equipped with a lanthanum hexaboride (LaB$_6$) crystal at a 200 kV accelerating voltage, a charge-coupled device (CCD) Gatan Orius SC200D for conventional imaging and diffraction, and a CCD Gatan UltraScan 1000XP for high-resolution imaging. For energy-dispersive X-ray (EDX) spectroscopy, a silicon drift detector (SDD) Oxford X-Max 80T was used. The average AuNR length and width, with corresponding standard deviations, were determined by measuring the size of at least 100 AuNRs for each sample with the ImageJ software. For fringe spacing measurements, Fast Fourier Transform (FFT) was performed on the raw HRTEM images to establish periodicities using the ImageJ software.

ζ-Potential Measurement

Samples were characterized by ζ-potential measurements with a Malvern Zetasizer Ultra. AuNRs (100 µL, ~1 nM) were dispersed in ultrapure water to obtain 1 mL of suspension (~0.1 nM). Disposable folded capillary cells (Zetasizer Nano Series) were used as sample container

and measurements were performed at 25 °C in triplicates. The reported values are the average measured ζ-potential values.

Dynamic Light Scattering

Samples were characterized by dynamic light scattering (DLS) through non-invasive backscattering (NIBS 173°) with a Malvern Zetasizer Ultra. Measurements were performed at 25 °C using a refractive index of 1.54 for the AuNRs. AuNRs (100 µL, ~1 nM) were dispersed in ultrapure water to obtain 1 mL of suspension (~0.1 nM) in disposable 4 clear sides PMMA cuvettes, and DLS measurements were performed in quintuplicates and averaged.

Surface-Enhanced Raman Spectroscopy

A Renishaw inVia Qontor confocal Raman microscope was used for SERS analysis of AuNRs. A 785 nm excitation wavelength was used to collect the Raman data. A 50× magnification objective with a numerical aperture of 0.5 was used. The laser power on the sample was adjusted to avoid sample deformation or burning during measurements. Exposure time was 1 s, providing a good signal-to-noise ratio. Before running any measurement, the setup was calibrated by measuring the silicon peak (520.5 ± 1 cm^{-1}) from a standard reference. For sample preparation, AuNRs (10 µL, ~1 nM) were deposited on a stainless steel slide and water was then evaporated with a flow of nitrogen gas before performing analysis. Data was processed and analysed using Renishaw's WiRE software and involved cosmic ray removal, baseline correction, denoising and normalization.

X-ray Photoelectron Spectroscopy

XPS data have been collected by a NEXSA G2 (ThermoFischer Scientific) spectrometer using a monochromated Al Ka X-ray beam working at 1486.6 eV and using a spot size of 200 µm^2. Survey spectra (0–1000 eV) were acquired with an analyser pass energy of 200 eV (1 eV/step) while high resolution core level spectra used a pass energy of 50 eV (0.1 eV/step). The core level spectra were peak-fitted using the CasaXPS software, Ltd. Version 2.3.25PR1.0. U2 Tougaard or Shirley backgrounds were used for the spectral analysis. The peak areas were normalized by the manufacturer-supplied sensitivity factor ($S_{C1s} = 1$, $S_{Na1s} = 10.588$, $S_{O1s} = 2.88$, $S_{N1s} = 1.676$, $S_{Ag3d} = 22.13$, $S_{Au4f} = 20.735$, $S_{S2p} = 1.88$). The sample preparation for XPS consists of the deposit of 20 µL of concentrated AuNRs colloids (deposits of the sediments after 10 min centrifugation at 5000 rpm) onto silicon or ITO substrates, and the water is left to evaporate at room conditions before the insertion of the substrates in the introduction chamber

of the spectrometer. Survey spectra were recorded at three different locations and we did not observe any difference.

Determination of the AuNR concentration

The AuNR concentrations were determined using the method described by Hu et al.,[2] which correlates the AuNR concentration to their optical properties. The mass concentration of Au atoms (ρ_{Au}) can be determined from the optical density at 400 nm (OD_{400}), as it is not dependent on the dispersity and geometry of AuNRs, with the following equation (eqn (1)):

$$\rho_{Au} \ (\mu g \ mL^{-1}) = \frac{OD_{400}}{0.0103} \Leftrightarrow \rho_{Au} \ (g \ L^{-1}) = \frac{10 \ OD_{400}}{103} \quad (1)$$

By approximating AuNRs as cylinders terminated with two hemispheres, the average AuNR volume (V_{AuNR}) can be estimated by TEM images with the following equation (eqn (2)):

$$V_{AuNR} = \pi \left(\frac{W}{2}\right)^2 (L - W) + \frac{4}{3}\pi \left(\frac{W}{2}\right)^3 = \pi \frac{W^2}{4}\left(L - \frac{W}{3}\right) \quad (2)$$

with L the average AuNR length and W the average AuNR width. Therefore, the AuNR molar concentration (C_{AuNR}) can be calculated with the following equation (eqn (3)):

$$C_{AuNR} \ (mol \ L^{-1}) = \frac{\rho_{Au}}{d_{Au} \ N_A \ V_{AuNR}} = \frac{10 \ OD_{400}}{103 \ d_{Au} \ N_A \ \pi \frac{W^2}{4}\left(L - \frac{W}{3}\right)} \quad (3)$$

with N_A the Avogadro constant and d_{Au} the density of gold.

Cyanine5.5 conjugation quantification

The amount of Cyanine5.5 amine conjugated to AuNRs was obtained by UV-visible spectroscopy using the following method:

(i) The total absorbance at 684 nm was measured. It corresponds to the sum of the absorbance of the fluorophore and the absorbance of the AuNRs.

(ii) The contribution of the AuNRs at 684 nm was estimated with a curve fitting of the absorption spectrum.

(iii) The fluorophore contribution at 684 nm was calculated by subtracting (ii) from (i), and its concentration was obtained using the extinction coefficient at 684 nm

(198 000 L mol^{-1} cm^{-1}). The fluorophore amount was then calculated by multiplying its concentration with the total solution volume.

(iv) The amount of fluorophore adsorbed onto the AuNRs and not covalently conjugated was obtained by performing step (i), (ii) and (iii) with the data obtained from a control experiment performed in the absence of EDC/sulfo-NHS.

(v) The amount of covalently conjugated fluorophore was calculated by subtracting (iv) from (iii). The loading (amount of conjugated fluorophore per AuNR) was obtained by dividing the fluorophore amount with the AuNR amount.

Photothermal conversion efficiency calculation

The photothermal conversion efficiency (η) of the AuNRs was calculated according to the method described by Roper *et al.* (eqn (4)):[3]

$$\eta\ (\%) = 100 \times \frac{hS(T_{max} - T_{amb}) - Q_0}{I(1 - 10^{-A_\lambda})} \qquad (4)$$

where h is the heat transfer coefficient, S the heat transfer surface area, T_{max} the maximum temperature, T_{amb} the ambient temperature, Q_0 the heat dissipated by the solvent and cuvette, I the incident laser power, and A_λ the absorbance of the photothermal absorber at the irradiation wavelength. The maximum temperature of the AuNR-X$_4$C$_4$ suspension was 88.5 °C and ambient temperature was 21.7 °C, so the temperature change of the suspension was 66.8 °C. For ultrapure water, the maximum temperature was 22.1 °C and the ambient temperature was 17.4 °C, so the temperature change was 4.7 °C. The laser power was 2.356 W (3 W cm^{-2} over 0.785 cm^2 irradiated aperture). The absorbance of the AuNR-X$_4$C$_4$ suspension at 808 nm was 0.5026. To determine hS, a dimensionless parameter θ, termed driving force temperature, is introduced as follows (eqn (5)):

$$\theta = \frac{T - T_{amb}}{T_{max} - T_{amb}} \qquad (5)$$

The system time constant for heat transfer τ_s can then be calculated with the following equation (eqn (6)):

$$t = -\tau_s \ln(\theta) \qquad (6)$$

By plotting the cooling period as a function of the negative natural logarithm of the driving force temperature, we can extract τ_s as the slope of the resulting linear curve. For the AuNR-X_4C_4 suspension, it was determined as 470.36 s (Fig. S8B) and 439.10 s for ultrapure water (Fig. S9B). The value of hS was then obtained from the following equation (eqn (7)):

$$\tau_s = \frac{\sum_i m_i C_{p,i}}{hS} \qquad (7)$$

where $m_i C_{p,i}$ are the products of mass and heat capacity of system components i (water and glass cuvette, the contribution of colloidal gold was found to be negligible). There was 2.000 mL of aqueous solution so m_{water} is 2.000 g, and $C_{p,water}$ is 4.184 J g^{-1} °C^{-1}. The portion of the glass cuvette which was in contact with the liquid sample had an approximate volume of 1.274 cm^3, so m_{glass} is 3.30 g by considering the density of the optical glass which is 2.59 g cm^{-3}, and $C_{p,glass}$ is 0.783 J g^{-1} °C^{-1}.[4] Therefore, hS was deduced to be 23.3 mW °C^{-1} for the AuNR-X_4C_4 suspension and 24.9 mW °C^{-1} for ultrapure water. Q_0 was then calculated to be 0.117 W by multiplying the hS value for ultrapure water (24.9 mW °C^{-1}) with the corresponding difference between the maximum temperature and the ambient temperature (4.7 °C). Finally, by substituting corresponding values for each parameter in eqn (4), the photothermal conversion efficiency of AuNR-X_4C_4 was calculated to be 89% ± 3%. The photothermal conversion efficiencies of other AuNRs were calculated following the same method.

Supplementary Tables

Table S1. Reaction conditions optimization for the functionalization of AuNR-CTAB with $X_4C_4(N_2^+)_4$, optimal conditions are highlighted in green.

| Reaction conditions		Observation	Rationalization
pH	< 5	Reversible AuNR aggregation during reaction and poor AuNR stability	AuNR aggregation caused by protonation of carboxyl groups. This results in unexposed surfaces within aggregates, leading to inefficient ligand exchange
	5–6.5	Average AuNR stability	Reduced reactivity of diazonium groups in mildly acidic conditions leading to incomplete ligand exchange
	6.9–7.1	High AuNR stability	Efficient ligand exchange
	> 8	AuNR aggregation	Poor stability of AuNR-CTAB in basic conditions
OD_{LSPR}	> 2	AuNR aggregation	Increased AuNR proximity during ζ-potential inversion process
	≤ 2	High AuNR stability	Efficient ligand exchange while preserving AuNR colloidal stability
[CTAB]	< 0.1 mM	AuNR aggregation	Poor stability of AuNR-CTAB at low CTAB concentrations
	0.1 mM	High AuNR stability	Efficient ligand exchange
	≥ 1 mM	Poor AuNR stability	Inefficient ligand exchange due to high CTAB concentration
Temperature	20 °C	Average AuNR stability	Low CTAB aqueous solubility inhibiting its removal from the AuNRs surface
	35 °C	High AuNR stability	High CTAB aqueous solubility leading to its efficient removal from the AuNRs surface
NaOH addition	At once	AuNR aggregation	Sudden pH increase leading to AuNR-CTAB destabilization
	Stepwise	High AuNR stability	Efficient ligand exchange while preserving AuNR colloidal stability

Supplementary Figures
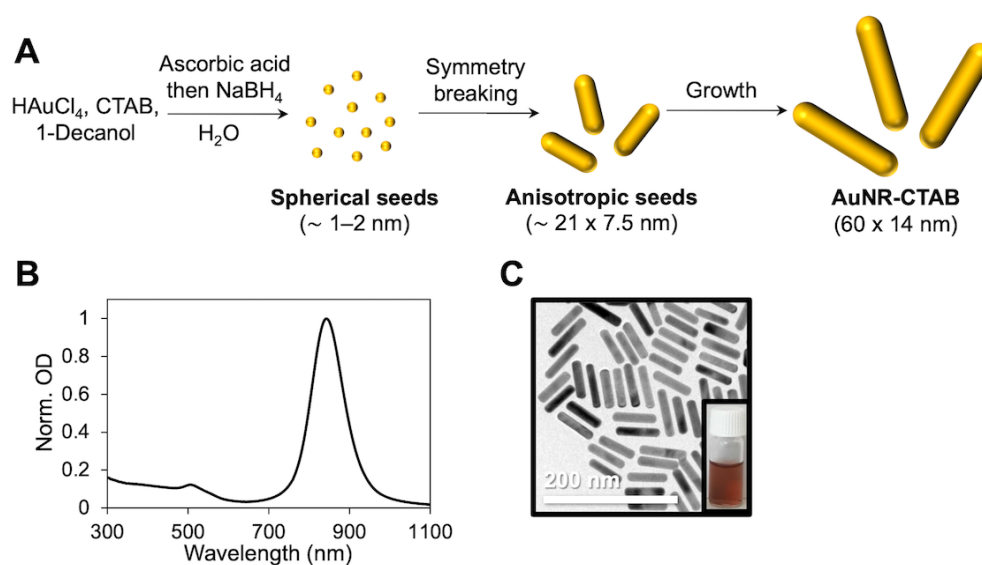
Fig. S1 AuNR-CTAB synthesis and characterization. (A) Simplified reaction scheme for the synthesis of AuNR-CTAB by decoupling the symmetry-breaking event from the seeded growth process. (B) UV-visible absorption spectra of as-synthesized AuNR-CTAB. (C) TEM image of as-synthesized AuNR-CTAB, the inset image shows the corresponding AuNR-CTAB suspension.
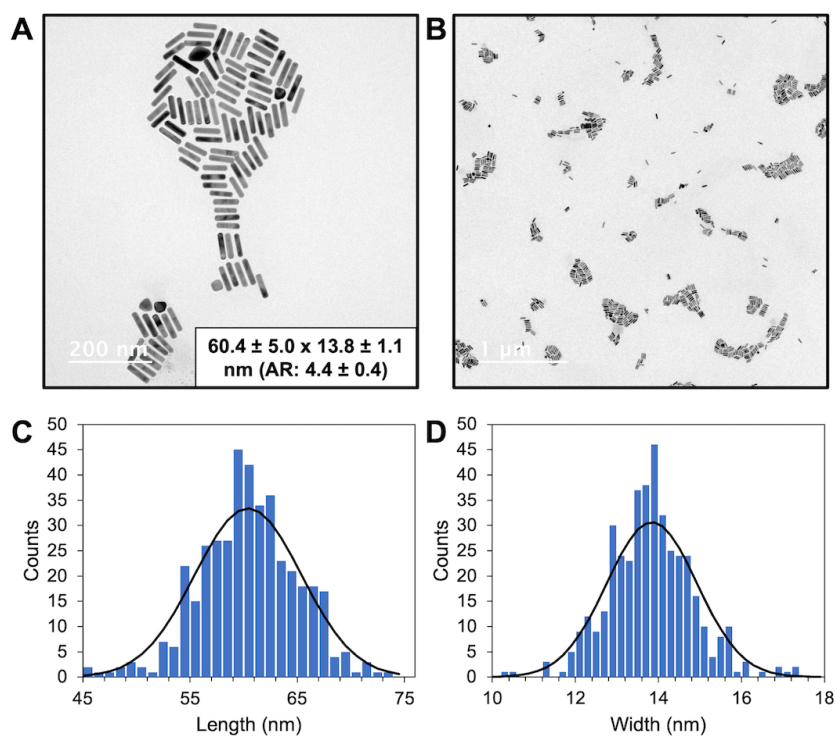

Fig. S2 (A, B) Enlarged TEM images of AuNR-CTAB with corresponding measured length (C) and width (D) distributions.
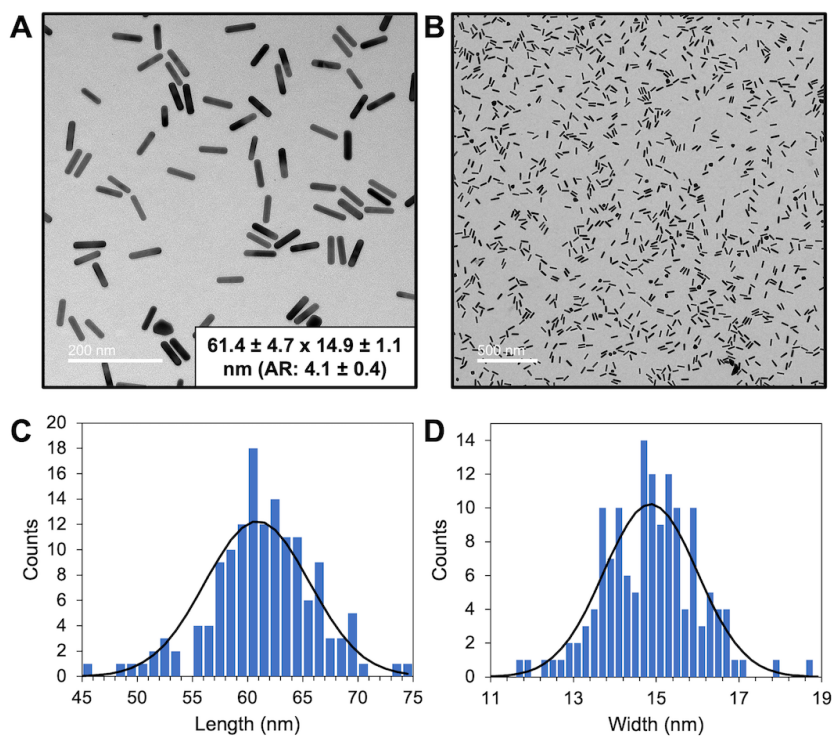
Fig. S3 (A, B) Enlarged TEM images of AuNR-X_4C_4 with corresponding measured length (C) and width (D) distributions.
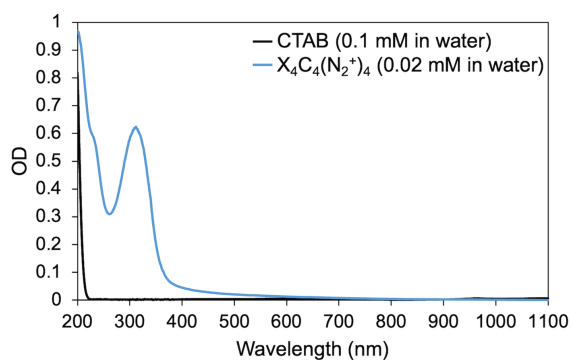
Fig. S4 UV-visible absorption spectra of CTAB (0.1 mM in water, black line) and $X_4C_4(N_2^+)_4$ (0.02 mM in water, blue line) solutions.
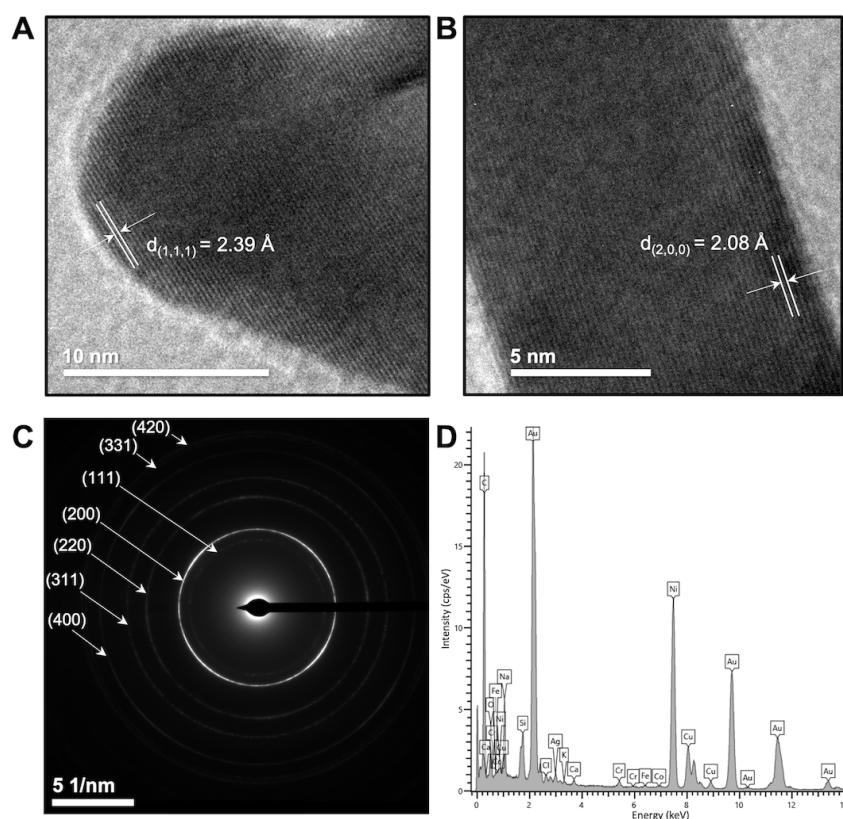
Fig. S5 (A, B) HRTEM images of AuNR-X$_4$C$_4$ showing a fringe spacing of (A) 2.39 Å, characteristic of the (1,1,1) lattice plane of gold, and (B) 2.08 Å, characteristic of the (2,0,0) lattice plane of gold. (C) SAED pattern of AuNR-X$_4$C$_4$ confirming the presence of face centred cubic (FCC) gold. (D) EDX spectrum of AuNR-X$_4$C$_4$ displaying high abundances of gold and carbon. The nickel, copper and cobalt come from the grid used during the experiment, the grid also contributes to the presence of carbon due to the carbon coating. The silicon comes from the sensor window, and the chromium and iron come from the sample holder.
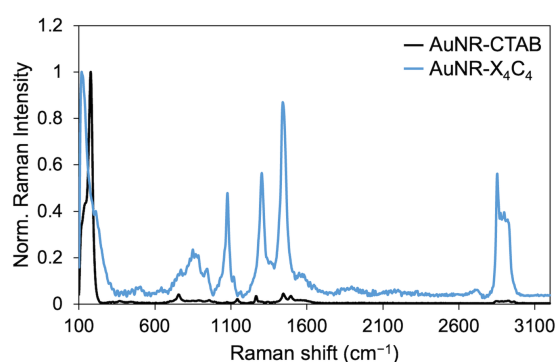
Fig. S6 Full range normalized SERS spectra of AuNR-CTAB (black line) and AuNR-X$_4$C$_4$ (blue line).
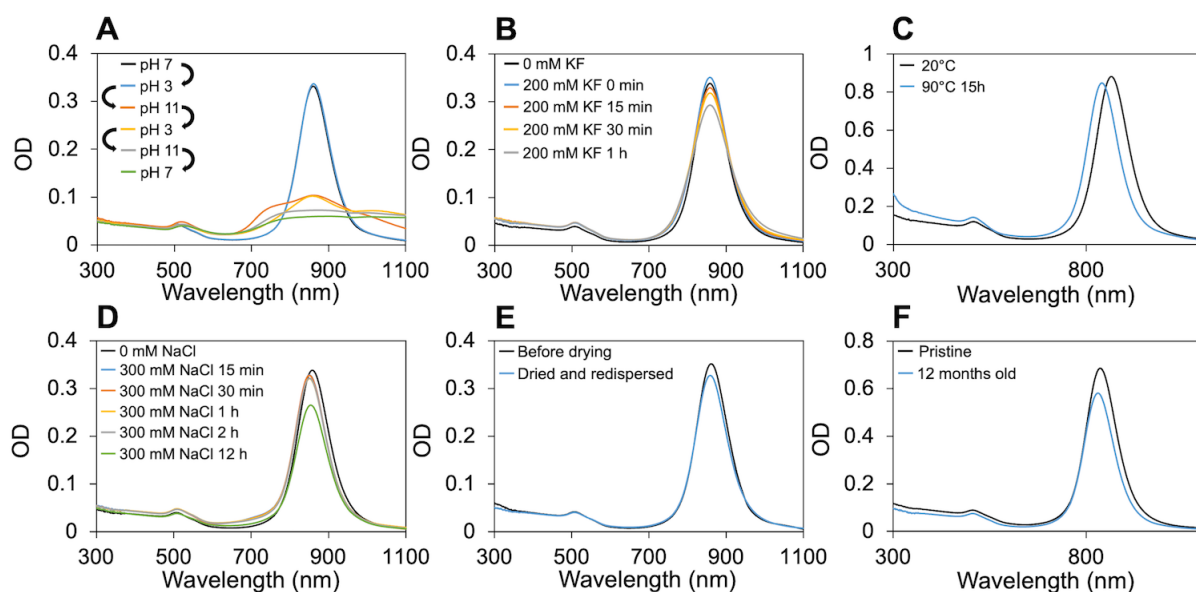
Fig. S7 Stability of AuNR-CTAB regarding (A) successive pH variations, (B) 200 mM KF incubation, (C) heating at 90 °C, (D) 300 mM NaCl incubation, (E) drying and resuspension, and (F) aging at room temperature.
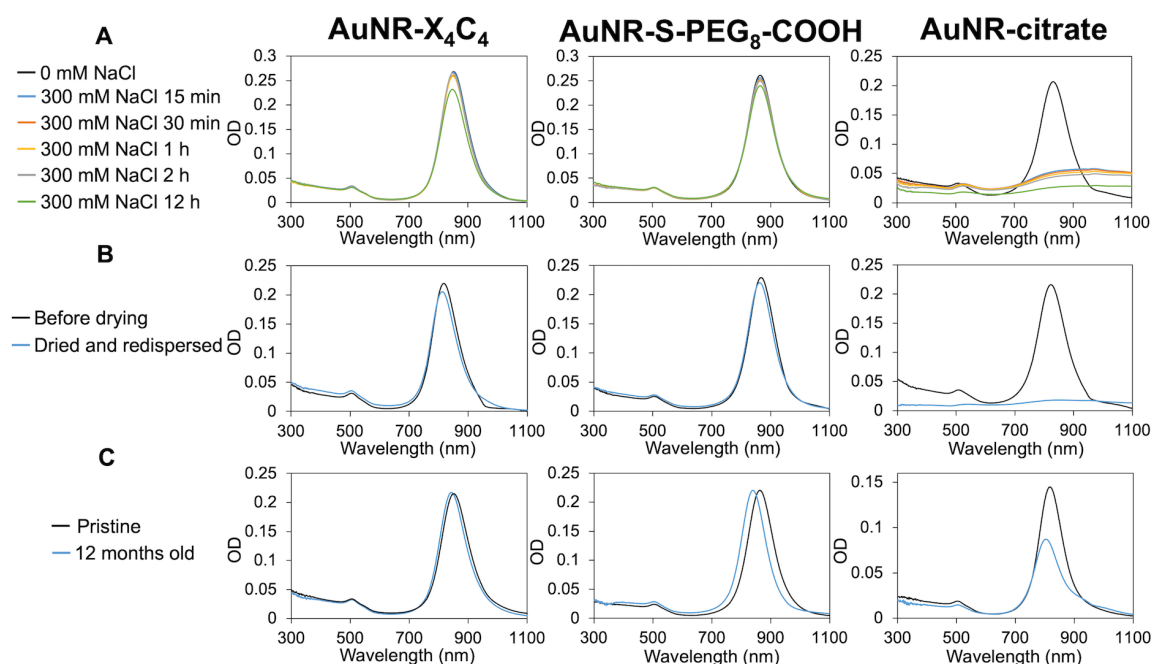
Fig. S8 Stability of AuNR-X_4C_4 (left), AuNR-S-PEG_8-COOH (middle) and AuNR-citrate (right) regarding (A) 300 mM NaCl incubation, (B) drying and resuspension, and (C) aging at room temperature.
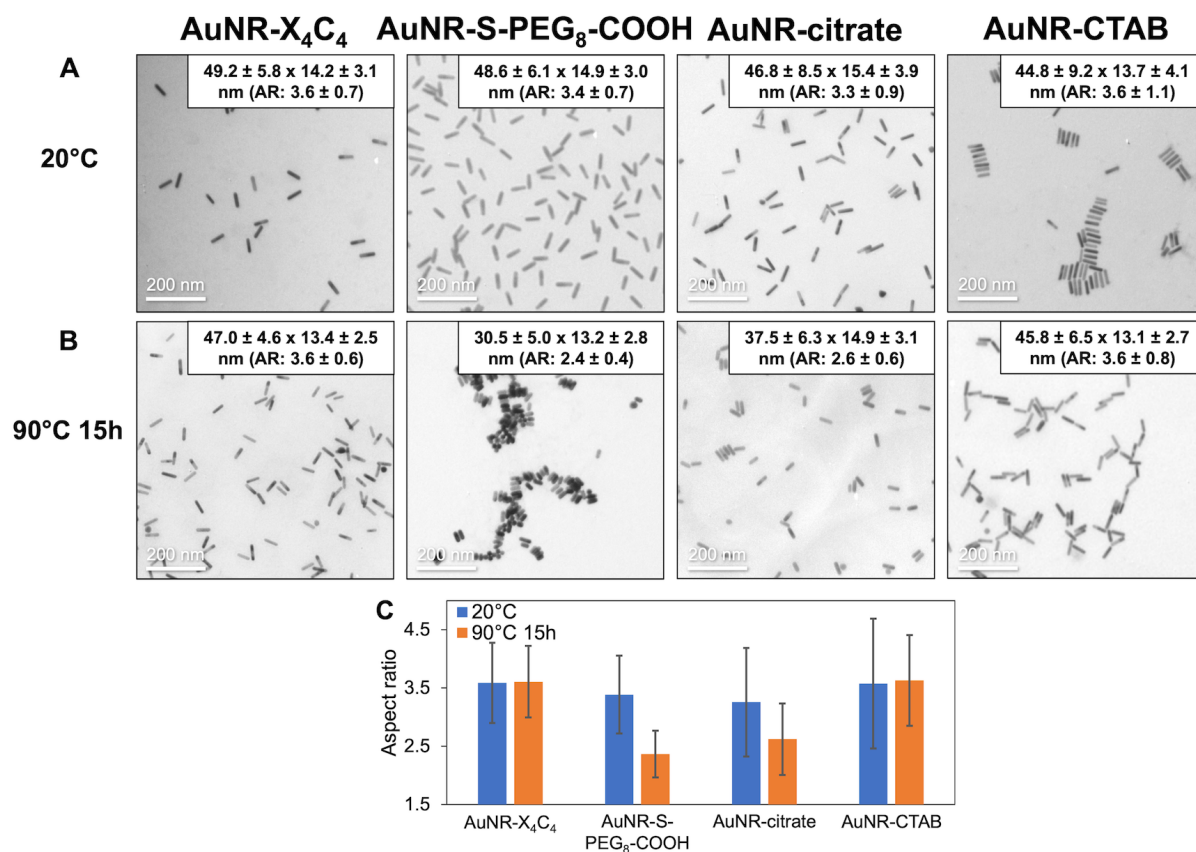
Fig. S9 TEM images of different AuNRs (A) before and (B) after heating at 90°C for 15 h. (C) AuNR aspect ratio variations measured by TEM before (blue) and after (orange) heating at 90°C for 15 h with standard deviation error bars. The reported aspect ratio values represent the averages calculated from more than 100 individual AuNR aspect ratio values measured from TEM images, except for AuNR-S-PEG$_8$-COOH after heating because the sample was too aggregated to analyse more than a few individual rods.
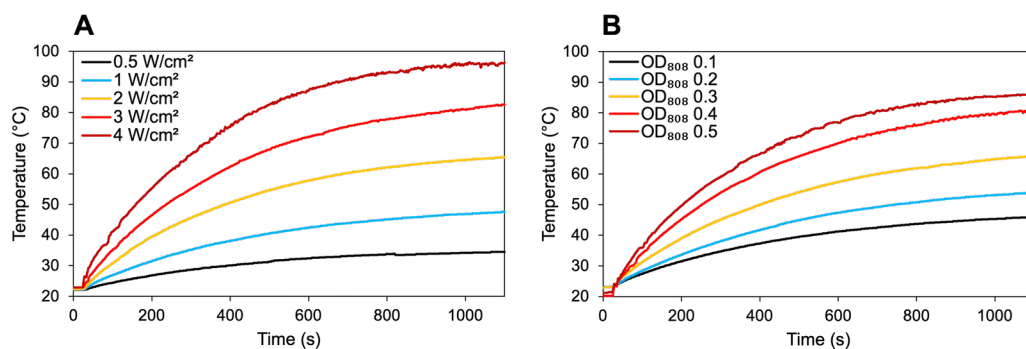
Fig. S10 Temperature profiles of aqueous solutions of AuNR-X$_4$C$_4$ with (A) varying power densities and fixed OD$_{808}$ (OD$_{808}$ = 0.5), or (B) varying OD$_{808}$ and fixed power density (3 W cm^{-2}).
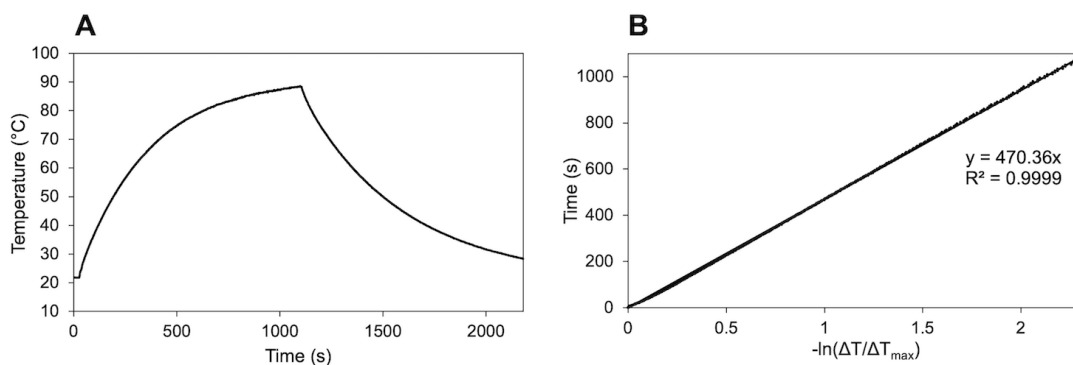
Fig. S11 (A) Temperature profile recorded on an aqueous solution of AuNR-X_4C_4 ($OD_{808} = 0.5$) when illuminated with an 808 nm laser (3 W cm^{-2}) for 18 min and after turning the laser off for 18 min. (B) Time from the cooling period (from 1080 to 2160 s) versus negative natural logarithm of the driving force temperature, with the associated linear trendline, equation and R^2 value.
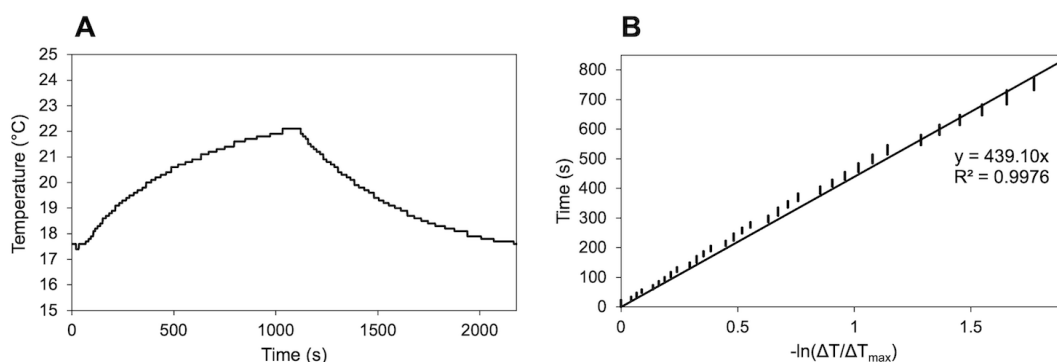

Fig. S12 (A) Temperature profile recorded on ultrapure water when illuminated with an 808 nm laser (3 W cm^{-2}) for 18 min and after turning the laser off for 18 min. (B) Time from the cooling period (from 1080 to 1919 s) versus negative natural logarithm of the driving force temperature, with the associated linear trendline, equation and R^2 value.
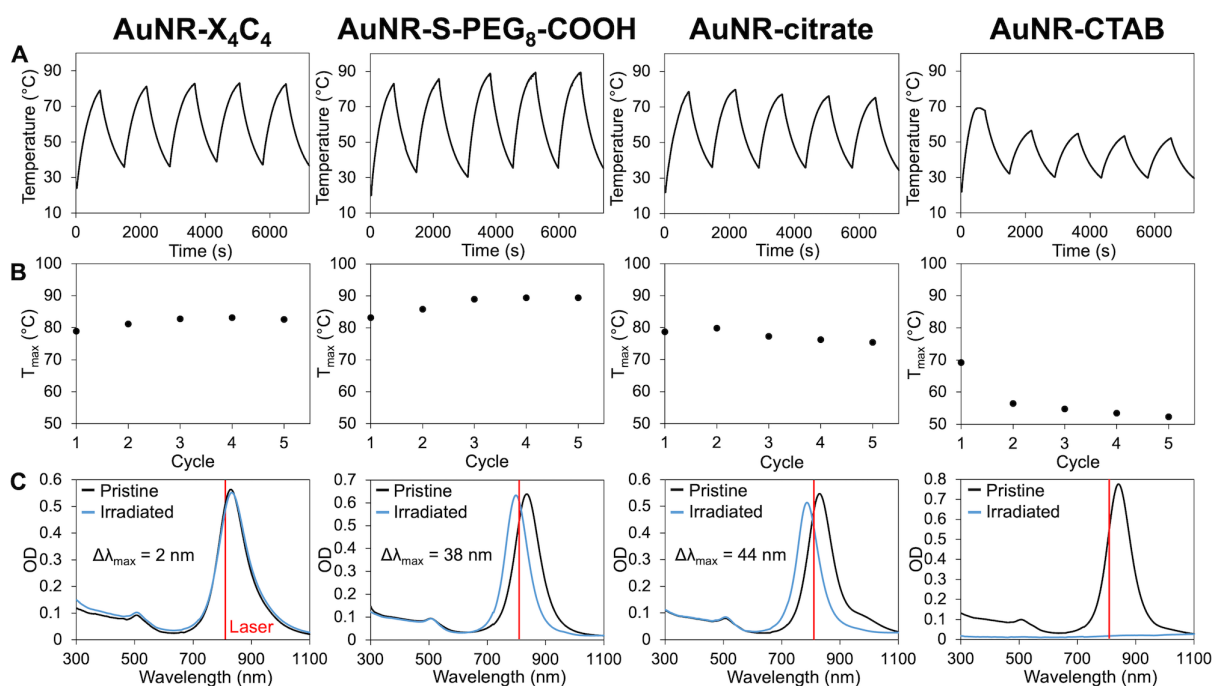
Fig. S13 Photothermal stability of different AuNRs over five consecutive heating/cooling cycles. (A) Temperature profiles recorded on aqueous solutions of AuNRs (OD_{808} = 0.5) when illuminated with an 808 nm laser (3 W cm^{-2}) for five consecutive heating/cooling cycles (12 min ON and 12 min OFF). (B) Maximum temperatures reached over five consecutive heating/cooling cycles. (C) UV-visible absorption spectra of AuNRs before (black line) and after (blue line) five consecutive heating/cooling cycles.
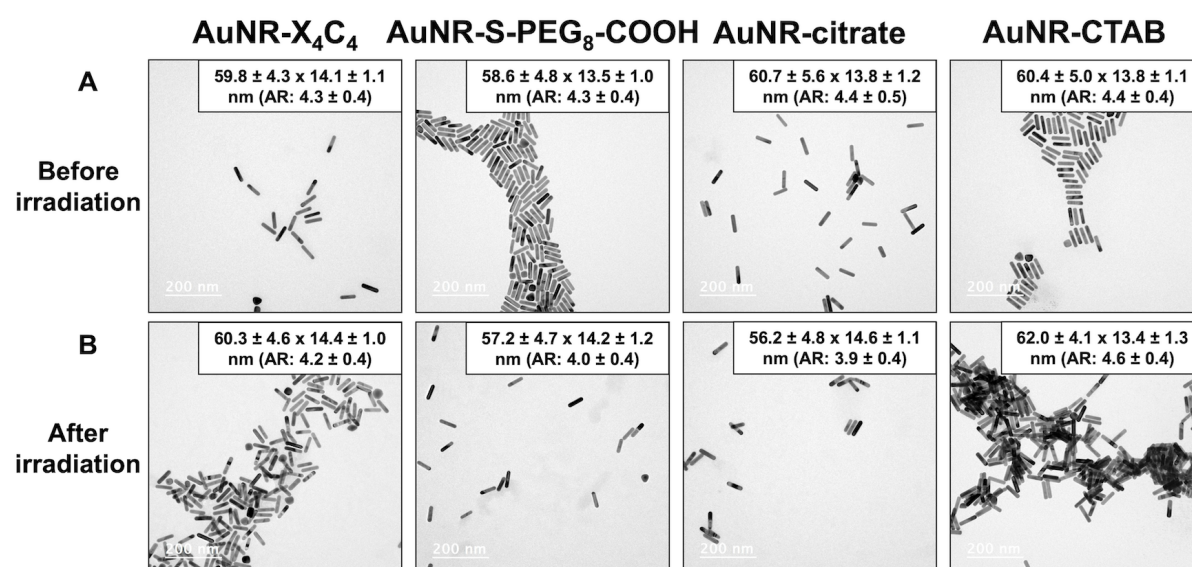

Fig. S14 TEM images of different AuNRs (A) before and (B) after irradiation with an 808 nm laser (3 W cm^{-2}) for 18 min.
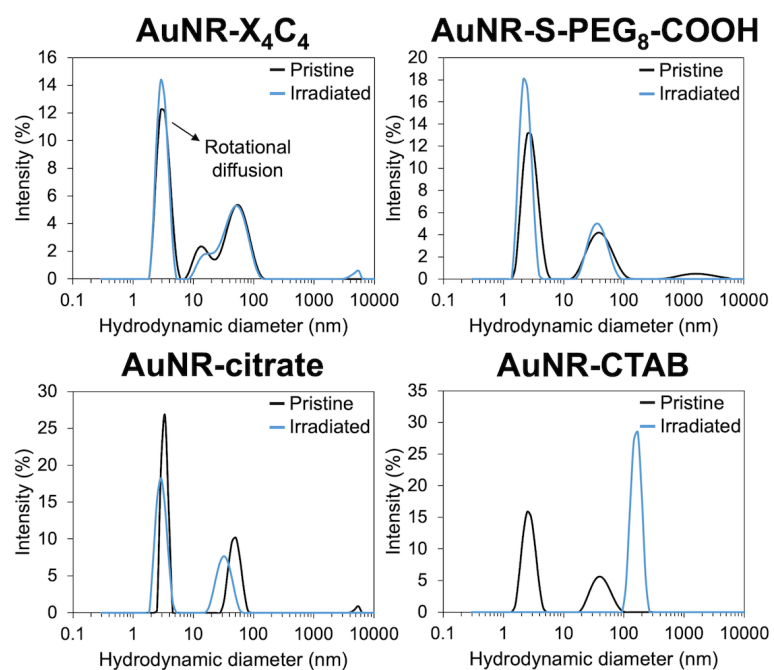
Fig. S15 DLS plots of different AuNRs before (black line) and after (blue line) irradiation with an 808 nm laser (3 W cm^{-2}) for 18 min.
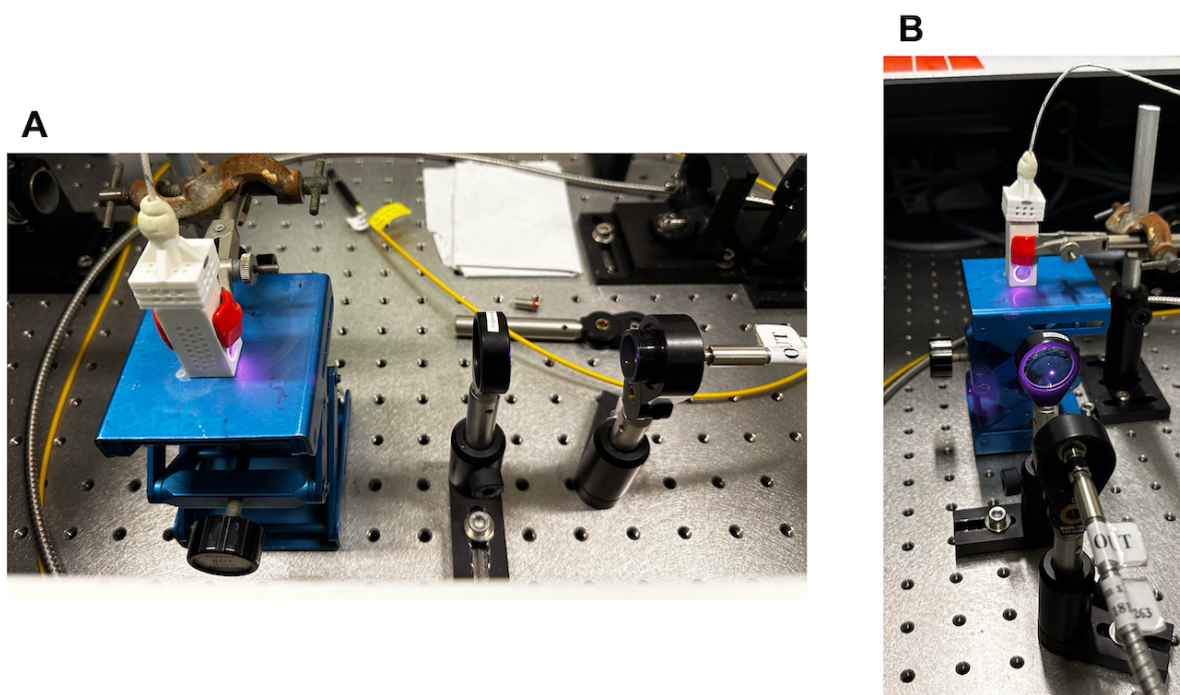

Fig. S16 Laser irradiation setup photographs from a (A) side view and (B) front view.
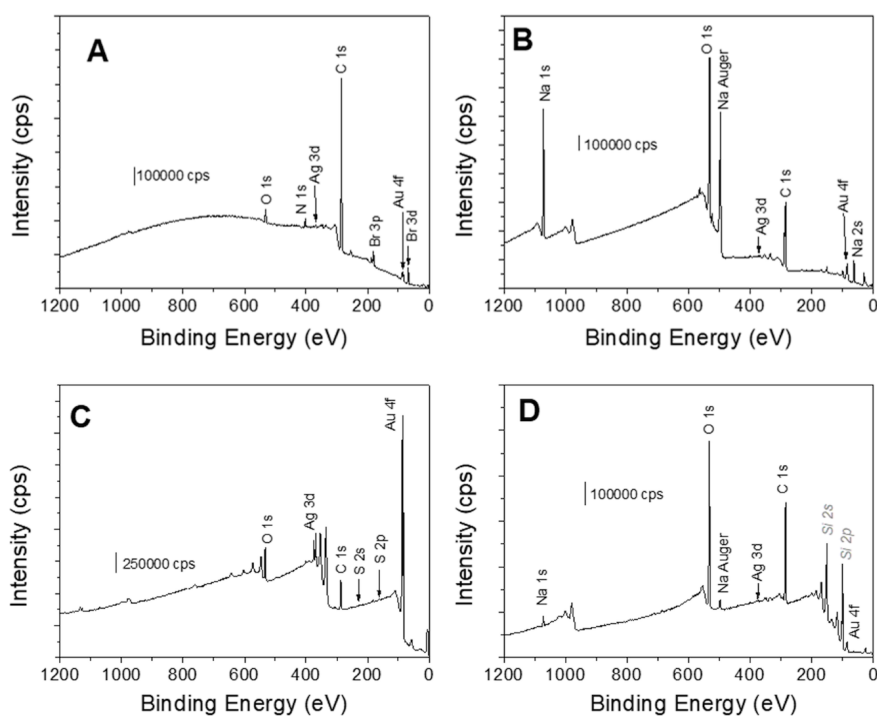
Fig. S17 XPS survey spectra of AuNR deposits onto Si (B,D) or ITO (A,C) substrates before laser irradiation for AuNR-CTAB (A), AuNR-citrate (B), AuNR-S-PEG$_8$-COOH (C) and AuNR-X$_4$C$_4$ (D). The XPS survey spectra (B-D) indicate the successful ligand exchange from CTAB, since bromine and nitrogen are not significantly distinguishable. A small contribution of silver could be observed in all spectra.
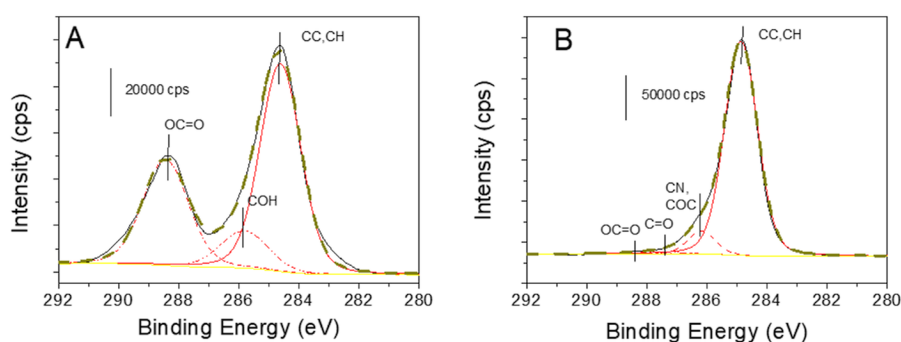

Fig. S18 High-resolution core level peak-fitted C 1s XPS spectra before laser irradiation for AuNR-citrate (A) and AuNR-CTAB (B). The C 1s signals and their corresponding fitting agree well with the molecular fingerprint of the capping agents, *i.e.* citrate and CTAB, respectively.
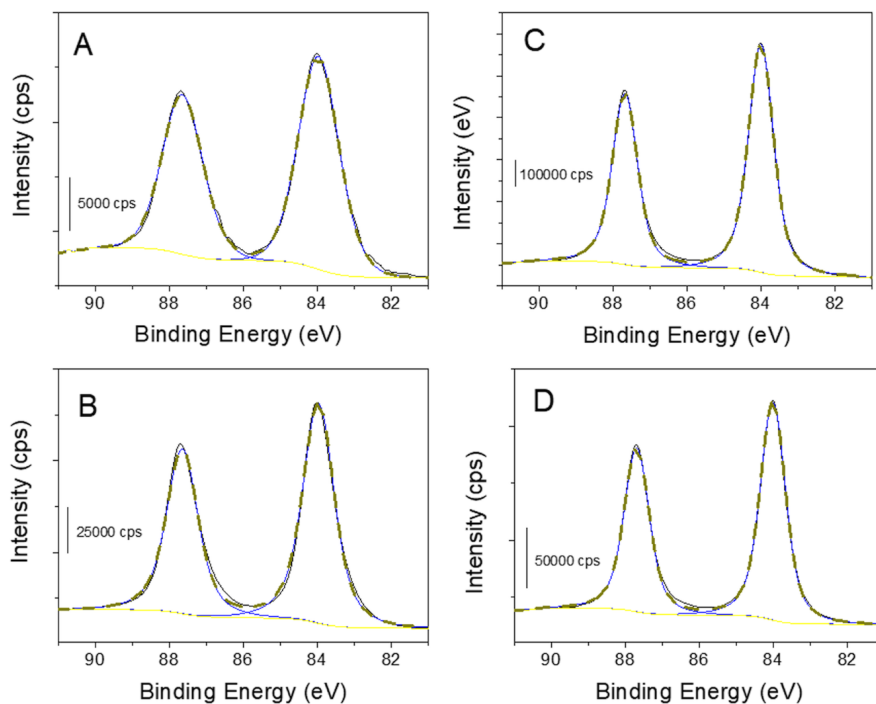
Fig. S19 High-resolution core level peak-fitted Au 4f XPS spectra before (A,C) and after (B,D) laser irradiation for AuNR-X$_4$C$_4$ (A,B) and AuNR-S-PEG$_8$-COOH (C,D). XPS data did not evidence any surface oxidation of the gold nanorods upon laser irradiation.

References

1   G. González-Rubio, V. Kumar, P. Llombart, P. Díaz-Núñez, E. Bladt, T. Altantzis, S. Bals, O. Peña-Rodríguez, E. G. Noya, L. G. Macdowell, A. Guerrero-Martínez and L. M. Liz-Marzán, *ACS Nano*, 2019, **13**, 4424–4435.

2   Z. J. Hu, S. Hou, Y. L. Ji, T. Wen, W. Q. Liu, H. Zhang, X. W. Shi, J. Yan and X. C. Wu, *AIP Adv.*, 2014, **4**, 117137.

3   D. K. Roper, W. Ahn and M. Hoepfner, *J. Phys. Chem. C*, 2007, **111**, 3636–3641.

4   Schott, *Data Sheet N-K5 522595.259*, .